Journal of Circuits, Systems, and Computers
Vol. 18, No. 4 (2009) 681–696

World Scientific
www.worldscientific.com

ON THE NONLINEAR MODELING OF RING OSCILLATORS

A. S. ELWAKIL
Department of Electrical and Computer Engineering,
University of Sharjah, P. O. Box 27272,
Sharjah, United Arab Emirates
elwakil@ieee.org

K. N. SALAMA
Electrical Engineering Department,
King Abdullah University of Science and Technology (KAUST),
Thuwal, Saudi Arabia
khaled_salama@ieee.org

Received 27 January 2009

We develop higher-order nonlinear models of three-stage and five-stage ring oscillators based on a novel inverter model. The oscillation condition and oscillation frequency are derived and compared to classical linear model analysis. Two important special cases for five-stage ring oscillators are also studied. Numerical simulations are shown.

Keywords: Ring oscillators; nonlinear oscillators; nonlinear circuits; nonlinear modeling.

1. Introduction

Ring oscillators are important blocks in many electronic systems.[1–3] For any oscillator, among other key parameters, finding the oscillation startup condition and oscillation frequency are the most important. Traditionally these are obtained via linearization with respect to the equilibrium point at the origin which allows an s-domain characteristic equation to be derived. Imposing the constraint that the characteristic equation has two pure imaginary roots yields the oscillation start-up and frequency formulae. However, linear analysis is not sufficient and fails to detect many undesired behaviors such as latchup, hysteresis jumps and chaos.[4–9]

In this work, we propose nonlinear models for three-stage and five-stage ring oscillators from which an interesting finding pertaining to the oscillation start-up condition is derived. We also model a practical five-stage ring oscillator with two shorts (known to reduce phase noise)[10] and explain in terms of effective system order why noise is reduced. Hysteresis and latch-up in this practical oscillator are also shown to be possible. We summarize the findings due to our nonlinear modeling

in the following points:

(a) The start-up oscillation condition for ring oscillators is found to be $A = +1$ where A is the loop gain. This is lower than the value obtained via linear analysis $A = +2$.
(b) The possibility of starting oscillations with a negative loop gain $A = -1$ is numerically confirmed. This is also associated with an oscillatory mode where the normalized oscillation frequency is $\omega_o = \sqrt{n}$; n is the number of stages in the ring oscillator rather than $\omega_o = 1/\sqrt{n}$ when $A = +1$ clearly indicating a possible increase in frequency by a factor of n times.
(c) A possible explanation for the lower phase noise in five stage ring oscillators with inter-stage short circuits[10] is given in terms of the effective oscillator state-space dimension.
(d) The possibility of predicting latch-up and chaos behaviors is demonstrated using one of the derived nonlinear models.

2. Digital-Inverter Model

Figure 1(a) shows the symbol of an inverter with a capacitor C_P connected between the inverter's input and output. This capacitor arises from unavoidable parasitics in the internal structure of the inverter such as the MOS transistor gate-to-drain capacitance C_{gd}. At low frequencies, this capacitor has a very high impedance and V_i is phase inverted while at very high frequencies it acts as a short circuit and hence V_i can no longer be inverted; i.e., V_i and V_o are in phase. This is typical for any inverter and implies a bandwidth within which the inverter properly introduces the required phase inversion. Figure 1(b) shows the proposed model for the inverter composed of a cascaded $-\tanh(\cdot)$ nonlinearity and an all-pass filter. The nonlinearity is described by $V_n = -V_{\text{sat}} \tanh(V_i/V_s)$; V_{sat} is a saturation voltage and V_s is used to adjust the internal slope; i.e., how sharp is the transition from V_{sat} to $-V_{\text{sat}}$. The all-pass filter, whose transfer function is $T(s) = (1 - Ts)/(1 + Ts)$, models the effect of C_P where $T = C_P r_{\text{out}}$ is the filter time constant and r_{out} is the output resistance of the inverter. The choice of the $\tanh(\cdot)$ nonlinearity is inspired by the fact that high speed digital inverters usually employ a Bipolar transistor differential pair where the relation between the input and output differential voltages is $V_{od} =$

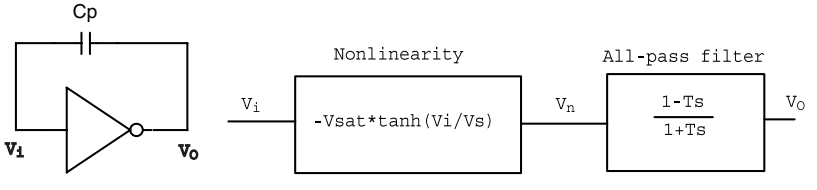

Fig. 1. (a) Digital inverter symbol with parasitic capacitor C_P and (b) proposed nonlinear model.

$-V_{\rm sat}\tanh(V_{id}/V_s)$.[3] If MOS transistors are used, a smooth $\sqrt{(\cdot)}$ function replaces the $\tanh(\cdot)$ nonlinearity with no significant qualitative difference. The following differential equation thus models the behavior of an inverter

$$V_o + T\dot{V}_o = -V_{\rm sat}\tanh(V_i/V_s) + T\frac{V_{\rm sat}}{V_s}[1-\tanh^2(V_i/V_s)]\dot{V}_i\,. \tag{1}$$

Introducing the dimensionless variables $x = V_i/V_{\rm ref}$, $y = V_o/V_{\rm ref}$, $\alpha = V_{\rm ref}/V_s$ and $\beta = V_{\rm sat}/V_{\rm ref}$, the above equation transforms into

$$y + \dot{y} = -\beta\tanh(\alpha x) + \alpha\cdot\beta[1-\tanh^2(\alpha x)]\dot{x}\,, \tag{2}$$

where time is normalized with respect to T and $V_{\rm ref}$ is an arbitrary reference voltage. Note that $\alpha\cdot\beta = V_{\rm sat}/V_s$ actually defines the internal gain A of the inverting amplifier (e.g., common-source amplifier or differential amplifier) used to realize the inverter. In particular, the higher the gain A, the sharper the inverter $V_i - V_o$ transfer characteristics become. Figure 2 is a plot of $y(t)$ when $x(t) = 1\sin(2000\pi t)$ obtained from numerical simulation of Eq. (2) in the two cases $(\alpha,\beta) = (-1,1)$ (upper subplot) and $(\alpha,\beta) = (-100,1)$ (lower subplot) respectively. The lower

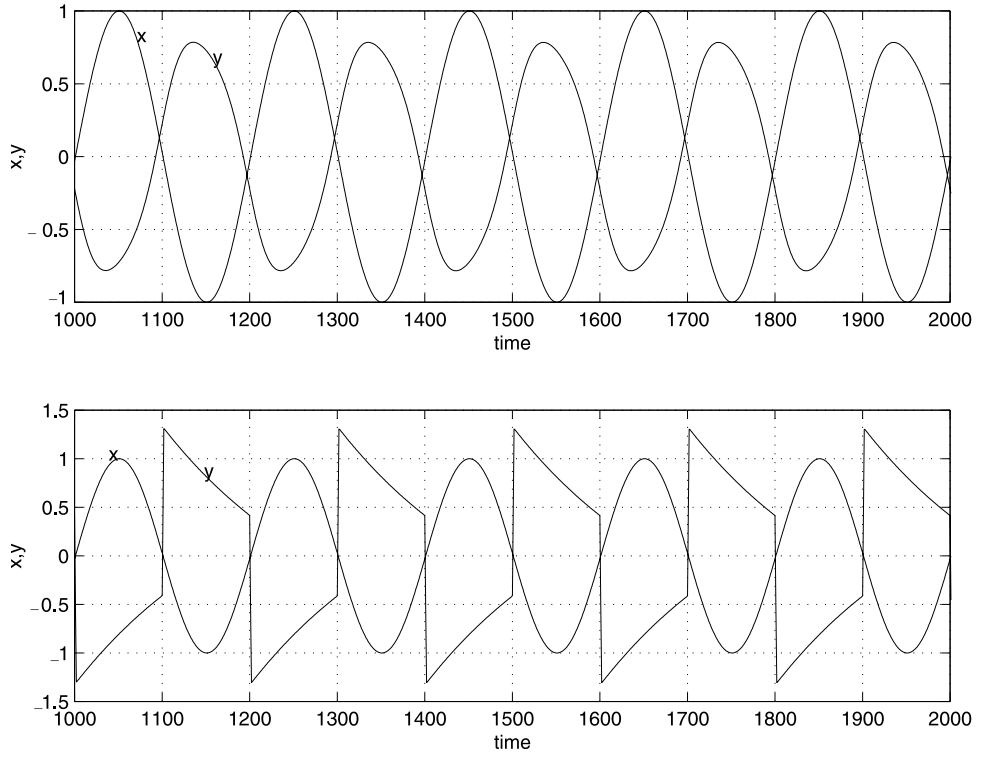

Fig. 2. Numerical simulations of the inverter nonlinear model of (2) in the two cases $\alpha = -1$ and $\alpha = -100$ ($\beta = 1$).

subplot corresponds to sharp inverter switching characteristics ($\alpha\beta = -100$) which is clear from the output waveform $y(t)$.

3. Ring Oscillators

3.1. *Three-stage oscillator*

Consider a ring oscillator formed of three cascaded inverters in a closed loop. Each inverter can be modeled as in Fig. 1(b) and hence, the overall system is described by

$$\dot{x} = -x - \beta \tanh(\alpha z) + \alpha\beta\dot{z}[1 - \tanh^2(\alpha z)]\,, \tag{3a}$$

$$\dot{y} = -y - \beta \tanh(\alpha x) + \alpha\beta\dot{x}[1 - \tanh^2(\alpha x)]\,, \tag{3b}$$

$$\dot{z} = -z - \beta \tanh(\alpha y) + \alpha\beta\dot{y}[1 - \tanh^2(\alpha y)]\,, \tag{3c}$$

where x, y and z are respectively the normalized outputs of the three inverters. In order to derive a condition for oscillation and estimate the oscillation frequency, we linearize the above system around the origin and separate variables to obtain

$$\dot{x} = \frac{1+A^3}{A^3-1}x + \frac{2A^2}{A^3-1}y + \frac{2A}{A^3-1}z\,, \tag{4a}$$

$$\dot{y} = \frac{2A}{A^3-1}x + \frac{1+A^3}{A^3-1}y + \frac{2A^2}{A^3-1}z\,, \tag{4b}$$

$$\dot{z} = \frac{2A^2}{A^3-1}x + \frac{2A}{A^3-1}y + \frac{1+A^3}{A^3-1}z\,, \tag{4c}$$

where the gain $A = \alpha \cdot \beta$. It can be shown that two pure imaginary eigenvalues and a zero real eigenvalue are admitted if A satisfies the relation

$$A^9 - A^6 - A^3 + 1 = 0\,, \tag{5}$$

for which the trivial solutions are $A = \pm 1$. Therefore, there are actually **two** possible conditions for oscillation. It is important here to comment on the implications of the condition $A = -1$. This condition means that the $\tanh(\cdot)$ nonlinearity has a positive slope around the origin. Thus, we do not have an inverter but rather a buffer at low frequencies ($\omega \ll \omega_T = 1/T$). However, note that due to the all-pass filter, phase inversion will take place in this buffer at very high frequencies ($\omega \gg \omega_T$). In other words, two types of inverters can be used to construct a ring oscillator; the first type is the classical inverter ($A = 1$) which provides 180° phase inversion at DC but fails to do so at high frequencies (due to the parasitic capacitor C_p). The second type ($A = -1$) provides near 180° phase inversion at very high frequencies while at DC it provides 0° phase shift meaning that it is a buffer. To the best of the authors knowledge, this possibility of constructing a ring oscillator using this special buffer is not known to circuit designers and is yet to be demonstrated.

It is important here to compare the results obtained from our nonlinear model with those which are traditionally obtained from a simple linear model. It is usually adopted that an inverter can be modeled as in inverting transconductor stage $(-g_m)$ driving a parallel RC load.[1] This leads to the one pole model $v_o/v_i = A/1 + TS$, where $A = g_m R$. Forming a three-stage ring oscillator with this model results in the characteristic equation $(1 - (A/1 + TS)^3 = 0)$ for which the oscillation condition is $A = 2$. The linear model not only fails to predict the negative gain possibility but also indicates a higher than necessary gain value to start oscillations $(A = 2)$.

Numerical simulations of Eq. (3) are shown in Figs. 3(a) and 3(b) for $A = \pm 1.05$. The $A\tanh(\alpha x)$ nonlinearity in the two cases is also plotted in Fig. 3(c). It is necessary to slightly increase A in order to start oscillations.

Assuming $A = 1 + \epsilon$ $(\epsilon \to 0)$, it can be shown that the characteristic equation of the linearized system under this oscillation condition is

$$3\epsilon\lambda^3 - (6 + 9\epsilon)\lambda^2 + \epsilon\lambda - 3\epsilon - 2 = 0\,, \tag{6}$$

which at $\epsilon \to 0$ reduces to $\lambda^2 + 1/3 = 0$. Hence the normalized frequency of oscillation is ideally $\omega_o = 1/\sqrt{3}$ (recall that time is normalized with respect to T). Alternatively, for $A = -(1 + \epsilon)$, it can be shown that the characteristic equation becomes

$$(2 + 9\epsilon)\lambda^3 - 9\epsilon\lambda^2 + (6 + 27\epsilon)\lambda - 3\epsilon = 0\,, \tag{7}$$

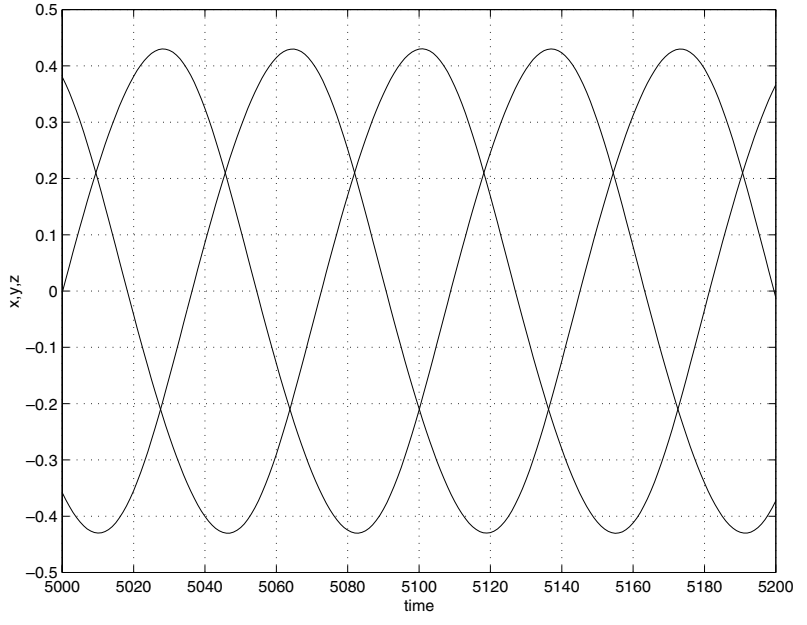

(a)

Fig. 3. Numerical simulations of (3). (a) $A = 1.05$, (b) $A = -1.05$ and (c) plot of the nonlinearity $A\tanh(\alpha x)$ in the two cases.

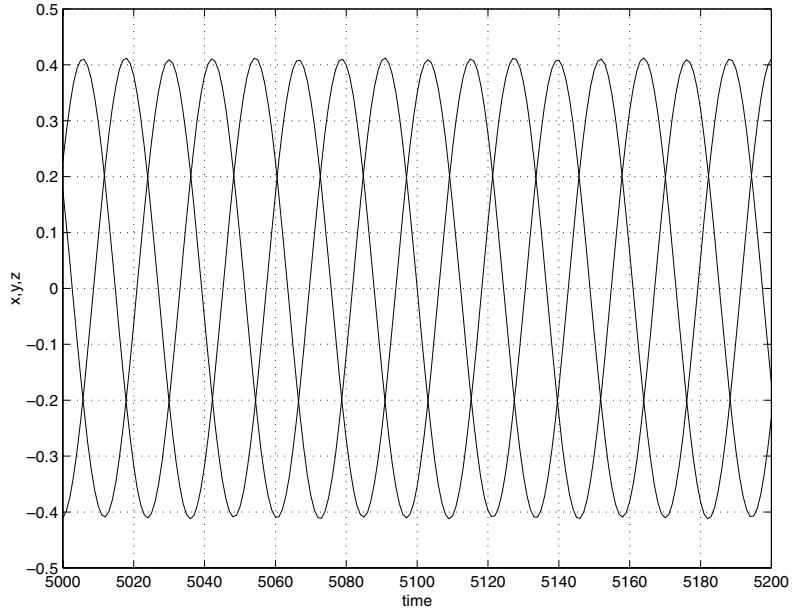

(b)

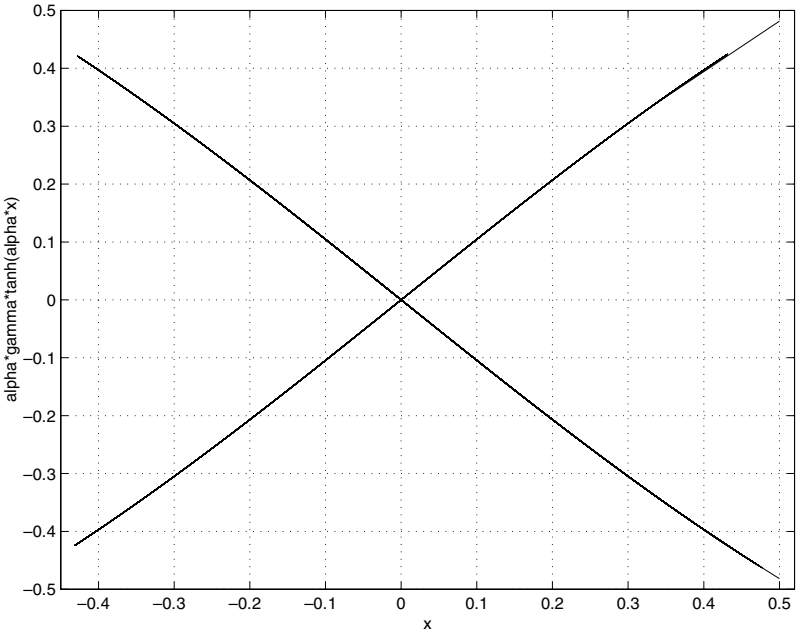

(c)

Fig. 3. (*Continued*)

which at $\epsilon \to 0$ reduces to $\lambda^3 + 3\lambda = 0$. Hence, the normalized oscillation frequency is ideally $\omega_o = \sqrt{3}$. It is clear that the oscillation frequency obtained by using the oscillation condition $A = -1$ is **three** times that obtained by using the condition $A = +1$, as is confirmed by the numerical simulations in Figs. 3(a) and 3(b).

3.2. *Five-stage oscillator*

In a similar manner, a five-stage ring oscillator can be modeled in which case the condition for oscillation is also found to be $A = \pm 1$ and the frequency of oscillation is either $\omega_o = 1/\sqrt{5}$ or $\omega = \sqrt{5}$, depending on which condition is satisfied. However, a practical five-stage ring oscillator may be implemented as shown in Fig. 4(a) where the outputs of the first (respectively second) and third (respectively fourth) stages are sorted. This practical implementation is known to reduce phase noise which is readily high for ring oscillators when compared to their LC counterparts by offering negative feedback.[10] To model this oscillator, it is important to recall that a monotone voltage-controlled cubic-type negative nonlinear resistor can be realized using two digital inverters, as shown in Fig. 4(b).[11] This voltage-controlled nonlinear resistor is modeled by

$$I_n = -\frac{V_n}{R_a} + \left(\frac{V_n}{R_b}\right)^3, \tag{8}$$

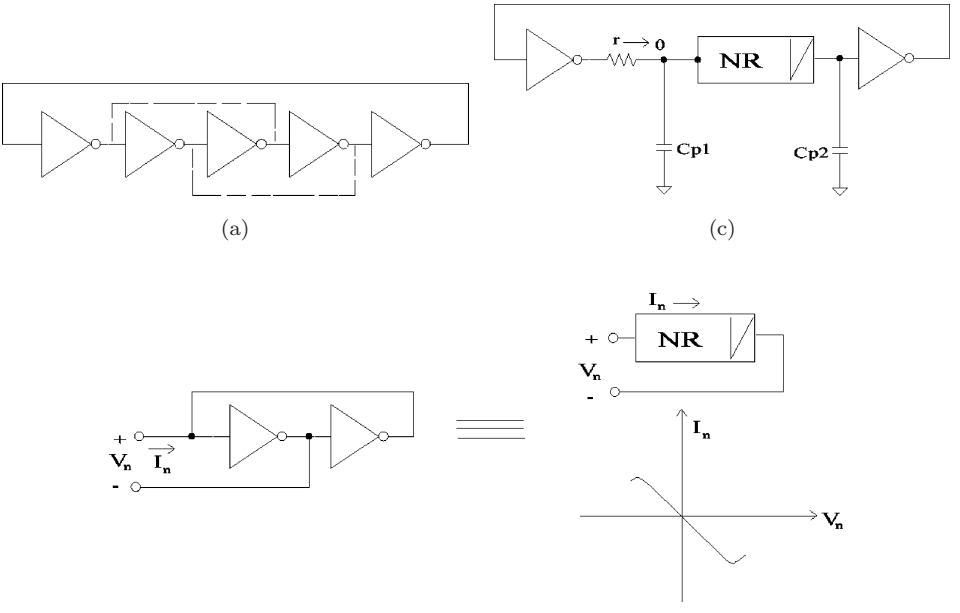

Fig. 4. Five-stage ring oscillator with two short circuits and its nonlinear equivalent circuit.

where $R_{a,b}$ are used to adjust the inner and outer slopes of this nonlinearity. It is clear that the first-third and second-fourth inverter pairs in Fig. 4(a) form two parallel nonlinear resistors which is effectively equivalent to a single cubic-type nonlinear resistor with slope adjusting resistors $0.5R_a$ and $0.5R_b$. Hence, this ring oscillator can be modeled as in Fig. 4(c). The two parasitic capacitors C_{P1} and C_{P2} are necessary to hold the voltage across the nonlinear resistor and must be included in the model. The modeling equations are

$$V_{o1} + T\dot{V}_{o1} = -V_{\rm sat}\tanh(V_{o2}/V_s) + TV_{\rm sat}\dot{V}_{o2}[1-\tanh^2(V_{o2}/V_s)]/V_s\,, \tag{9a}$$

$$V_{o2} + T\dot{V}_{o2} = -V_{\rm sat}\tanh(V_{C_{P2}}/V_s) + TV_{\rm sat}\dot{V}_{C_{P2}}[1-\tanh^2(V_{C_{P2}}/V_s)]/V_s\,, \tag{9b}$$

$$rC_{P1}\dot{V}_{C_{P1}} = V_{o1} - V_{C_{P1}} - rI_n\,, \tag{9c}$$

$$C_{P2}\dot{V}_{C_{P2}} = I_n\,. \tag{9d}$$

Note that it is also necessary to include the parasitic resistor r ($r \to 0$) (see Fig. 4(c)) otherwise the state variable $V_{C_{P1}}$ will coincide with the state variable V_{o1}, where $V_{o1,2}$ are the outputs of the two inverters shown in Fig. 4(c) and I_n is as given by Eq. (8).

Introducing the dimensionless variables $x = V_{o1}/V_{\rm ref}$, $y = V_{o2}/V_{\rm ref}$, $z = V_{C_{P1}}/V_{\rm ref}$, $w = V_{C_{P2}}/V_{\rm ref}$, $\varepsilon = rC_{P1}/T$, $b = r/R_a$, $c = r/R_b$ and assuming for simplicity $C_{P1} = C_{P2}$, the above equations transform into

$$\dot{x} = -x - \beta\tanh(\alpha y) + \alpha\beta\dot{y}[1-\tanh^2(\alpha y)]\,, \tag{10a}$$

$$\dot{y} = -y - \beta\tanh(\alpha w) + \alpha\beta\dot{w}[1-\tanh^2(\alpha w)]\,, \tag{10b}$$

$$\varepsilon\dot{z} = x - z - f(w-z)\,, \tag{10c}$$

$$\varepsilon\dot{w} = f(w-z)\,, \tag{10d}$$

where α and β are as defined before and the nonlinearity $f(w-z)$ is given by

$$f(w-z) = -b(w-z) + c(w-z)^3\,. \tag{11}$$

Note that since $r \to 0$ so $\varepsilon \to 0$ which indicates that the above system of differential equations is stiff and that the oscillator is effectively living in a two-dimensional subspace, rather than a five-dimensional space, when compared to a classical five-stage ring oscillator. Recalling basic knowledge of nonlinear dynamical systems, the higher the order of the system the higher its capacity to generate noise (or chaos). In fact, an ideal white-noise source has infinite dimension. It is thus easy to understand why the five-stage ring oscillator of Fig. 4(a) has better phase-noise than the classical one and is more practically used. A straightforward approach to reduce the noise content of any system is to reduce its effective space dimension.

The above system of equations can be linearized around the origin as

$$\begin{pmatrix} \dot{x} \\ \dot{y} \\ \dot{z} \\ \dot{w} \end{pmatrix} = \begin{pmatrix} -1 & -2A & \dfrac{A^2 b}{\varepsilon} & -A^2\left(1+\dfrac{b}{\varepsilon}\right) \\ 0 & -1 & \dfrac{Ab}{\varepsilon} & -A\left(1+\dfrac{b}{\varepsilon}\right) \\ \dfrac{1}{\varepsilon} & 0 & \dfrac{-(1+b)}{\varepsilon} & \dfrac{b}{\varepsilon} \\ 0 & 0 & \dfrac{b}{\varepsilon} & \dfrac{-b}{\varepsilon} \end{pmatrix} \begin{pmatrix} x \\ y \\ z \\ w \end{pmatrix}. \tag{12}$$

The characteristic equation is thus found to be

$$\begin{aligned} &\varepsilon^2\lambda^4 + \varepsilon(2\varepsilon + 2b + 1)\lambda^3 + (\varepsilon^2 + 2\varepsilon + 4b\varepsilon + b - A^2 b)\lambda^2 \\ &\quad + (\varepsilon + 2b\varepsilon + 2b + 2A^2 b)\lambda + b(1 - A^2) = 0\,, \end{aligned} \tag{13}$$

neglecting the ε^2 terms, the condition for having pure imaginary roots is found to be

$$A^2 = 0.5(q + \sqrt{q^2 + 4(1+q)})\,, \tag{14}$$

where $q = 2\varepsilon(1+2b)/b^2$. For $q \ll 1$, the above condition simply reduces to $A^2 = 1$; i.e., $A = \pm 1$, which is the same condition for oscillation of any classical ring oscillator.

Figure 5(a) represents the waveform obtained from numerical simulations[a] with $\alpha = 1.01$, $\beta = 1$, $\varepsilon = 0.001$ and $b = c = 0.5$. These values correspond to $q = 0.016$ and hence the minimum required value to start oscillations in this case is $A = 1.008$. The four roots of Eq. (13) are: $(0, -2005.5, 1.76 \pm j31.7)$ which clearly indicates two complex roots and the normalized frequency of oscillation is $\omega = 31.7$ (recall that time is normalized with respect to T). We may also express the condition for oscillation simply as $A = \pm(1+\epsilon)$. The larger the values of ϵ, the larger the real part of complex roots and hence the higher the distortion content in the generated signal. For example, the roots at $\epsilon = 0.05$ are $(0, -2025, 11.9 \pm j32)$. Thus increasing ϵ by 0.042 shifts the real part of the complex roots from $+1.76$ ($\epsilon = 0.008$) to $+11.9$ ($\epsilon = 0.05$). As an implication, and since such small errors in the gain A above its necessary value of ± 1 cannot be avoided even with excellent circuit design practice, designers should expect that the Total Harmonic Distortion (THD) of ring oscillators is relatively high, which is also well-known.[1,12]

[a]An adaptive-step fifth-order Runge-Kutta algorithm is used for Matlab simulations of this stiff system.[13] All simulations have a run-time < 2 minutes on a 1.86 GHz P4 processor except for the simulation in Fig. 5(c) which has a 10 minute run-time.

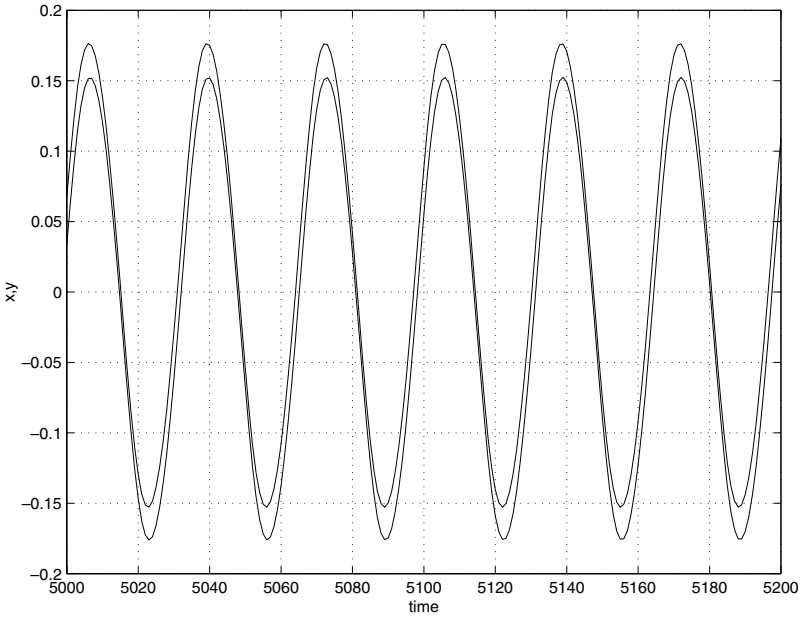

(a)

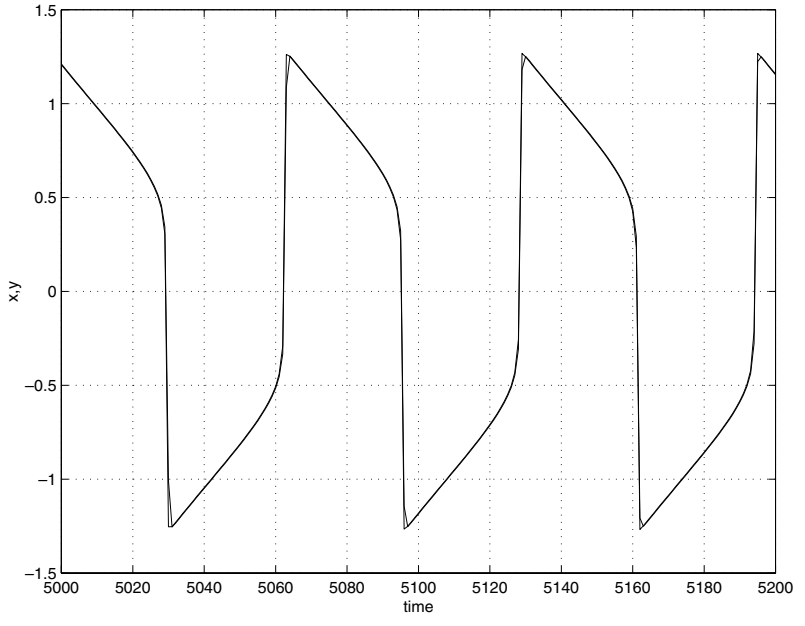

(b)

Fig. 5. Numerical simulation results of (10) with (a) $\epsilon = 0.001$ (sinusoidal oscillations), (b) $\epsilon = 1$ (relaxation oscillations), (c) $\varepsilon = 0.01$ (latchup) and (d) measuring the strength of the $\tanh(\cdot)$ nonlinearity (large excursion) and the cubic $f(w - z)$ nonlinearity (tiny excursion around the origin) during oscillations.

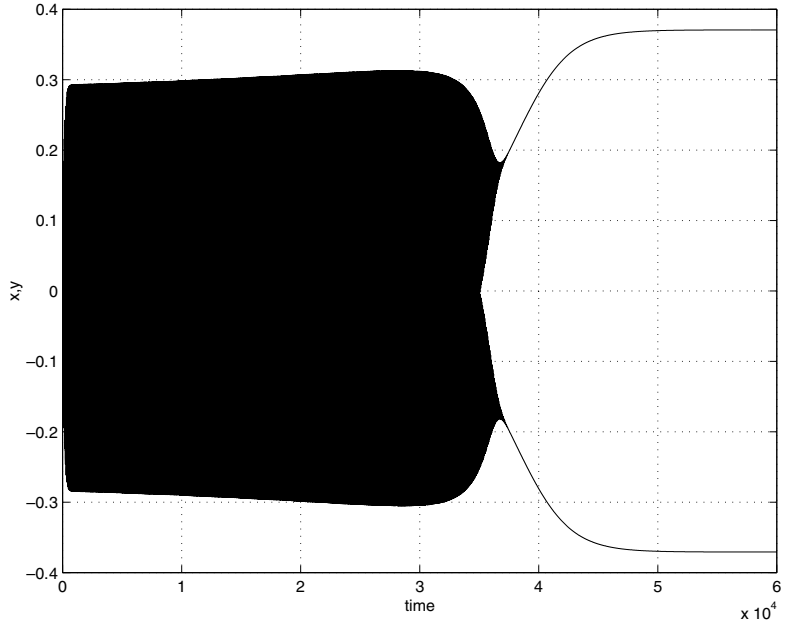

(c)

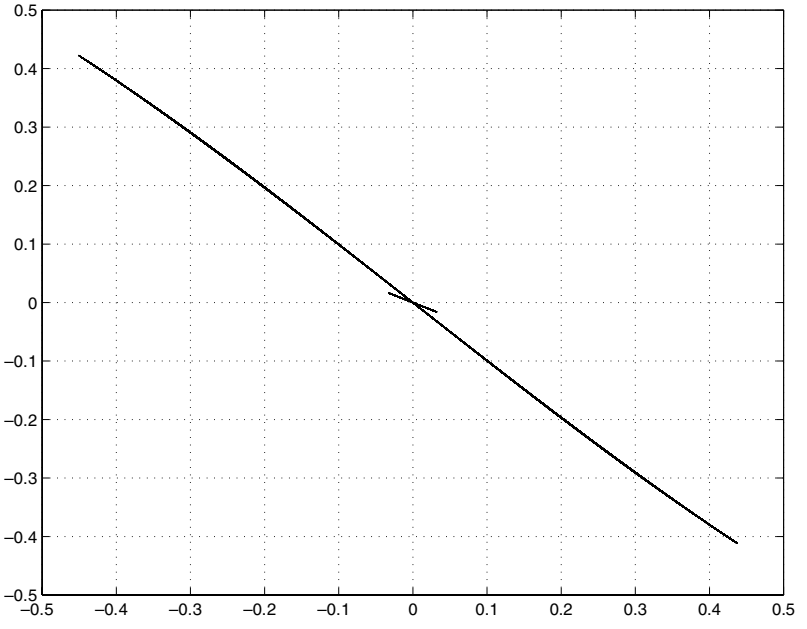

(d)

Fig. 5. (*Continued*)

We may also find the frequency of oscillation expression from Eq. (13) as

$$\omega_o = \sqrt{\frac{\varepsilon(1+2b)+2b(1+A^2)}{\varepsilon(1+2b+2\varepsilon)}} \approx \sqrt{\frac{4b(1+\epsilon)}{\varepsilon(1+2b)}}\,. \tag{15}$$

It is worth noting that the linearization of Eq. (12) is also limited by ϵ. For example, at $\epsilon = 1$, which is a too high error in the gain, Eq. (12) and hence Eq. (13) admits only four real roots two of which are positive. This will excite hysteresis[4,5] and the resulting waveforms are no longer sinusoids, as shown in Fig. 5(b). It is also worth noting that this oscillator may exhibit latchup as shown in Fig. 5(c) for $\varepsilon = 0.01$.[6,9] To verify the reason for this latchup, we need to derive a piecewise-linear model of this oscillator after measuring the strength of both the $\tanh(\cdot)$ nonlinearity and the cubic nonlinearity $f(w-z)$ under oscillatory conditions. Figure 5(d) clearly indicates the dominance of the $\tanh(\cdot)$ nonlinearity (large excursion) compared to the cubic-nonlinearity (tiny excursion). This means that the nonlinear resistor in Fig. 4 can be treated sufficiently as a linear negative resistor. Hence, the following piecewise-linear model can be derived

$$\begin{pmatrix}\dot{x}\\ \dot{y}\\ \dot{z}\\ \dot{w}\end{pmatrix} = \begin{pmatrix} -1 & -A-\beta m & \dfrac{b}{\varepsilon}A^2 & -A\left(\beta m+\dfrac{b}{\varepsilon}A\right)\\ 0 & -1 & \dfrac{b}{\varepsilon}A & -\dfrac{b}{\varepsilon}A-\beta m\\ \dfrac{1}{\varepsilon} & 0 & -\dfrac{1+b}{\varepsilon} & \dfrac{b}{\varepsilon}\\ 0 & 0 & \dfrac{b}{\varepsilon} & -\dfrac{b}{\varepsilon}\end{pmatrix}\begin{pmatrix}x\\ y\\ z\\ w\end{pmatrix} + \begin{pmatrix}-\beta n(1+A)\\ -\beta n\\ 0\\ 0\end{pmatrix}, \tag{16}$$

where

$$(m.n) = \begin{cases}(0,p) & y,\ w \geq \dfrac{p}{\alpha}\,,\\ (\alpha,0) & -\dfrac{p}{\alpha} < y,\ w < \dfrac{p}{\alpha}\,,\\ (0,-p) & y,\ w \leq -\dfrac{p}{\alpha}\,.\end{cases} \tag{17}$$

The factor p is used to adjust the location at which we assume saturation. For example, if we assume saturation is reached at $0.9V_{\text{sat}}$ then $p = \tanh^{-1}(0.9) \approx 1.5$. It is clear that the above system has three equilibrium points; one is the origin where $(m,n) = (\alpha, 0)$ and two others in the positive and negative saturation regions. The eigenvalue pattern at the origin with $\alpha = 1.008$, $\beta = 1$, $\varepsilon = 0.01$ and $b = 0.5$ (corresponding to the simulation of Fig. 5(c)) is $(+0.0038, -0.548 \pm j10.05, -200.9)$

indicating the appearance of one positive real eigenvalue; i.e., this equilibrium point is unstable. However, at any of the other two equilibrium points, the eigenvalue pattern is $(-0.4955, -0.4525 \pm j7.08, -200.6)$ indicating these two equilibria are stable and hence trajectories reaching them will settle indefinitely there causing latchup as shown in Fig. 5(c).[6,9]

3.2.1. *Five-stage oscillator with one short-circuit*

In the previous section we modeled the practical five-stage ring oscillator with two shorts. Here, we see what happens if only one short is maintained, as shown in Fig. 6(a). The short-circuit connection results in a well-known nonmonotone nonlinear resistor, as shown in Fig. 6(b).[14,15] Therefore, the oscillator may be modeled as in Fig. 6(c). Nonmonotone resistors give rise to hysteresis if the full range of the nonlinearity is covered.[4] However, this nonlinearity is weak and non-dominant when compared to the $\tanh(\cdot)$ nonlinearity, similar to the case plotted in Fig. 5(d). Hence, this nonlinear resistor can be considered only as a linear negative resistor R_n. In this case, the inverter labeled 2 in Fig. 6(c) along with the nonlinear resistor and the two parasitic capacitors C_P and C_{P1} can be modeled by a $-\tanh(\cdot)$ nonlinearity in cascade with a filter whose transfer function is $(1 - T_1 s)/(1 - T_2 s)$, as shown in Fig. 6(d). T_1 and T_2 are equal to $R_n(C_P + C_{P1})$ and $R_n C_P$ respectively. Inverters 1 and 3 may still be modeled as in Fig. 1.

Defining $k_1 = T_1/T$ and $k_2 = T_2/T$, this oscillator is then described by

$$\dot{x} = -x - \beta \tanh(\alpha z) + \alpha\beta[1 - \tanh^2(\alpha z)]\dot{z}\,, \tag{18a}$$

$$-k_2\dot{y} = -y - \beta \tanh(\alpha x) + \alpha\beta k_1[1 - \tanh^2(\alpha x)]\dot{x}\,, \tag{18b}$$

$$\dot{z} = -z - \beta \tanh(\alpha y) + \alpha\beta[1 - \tanh^2(\alpha y)]\dot{y}\,, \tag{18c}$$

where x, y and z correspond to the normalized output voltages of the three inverters respectively and α, β are as previously defined.

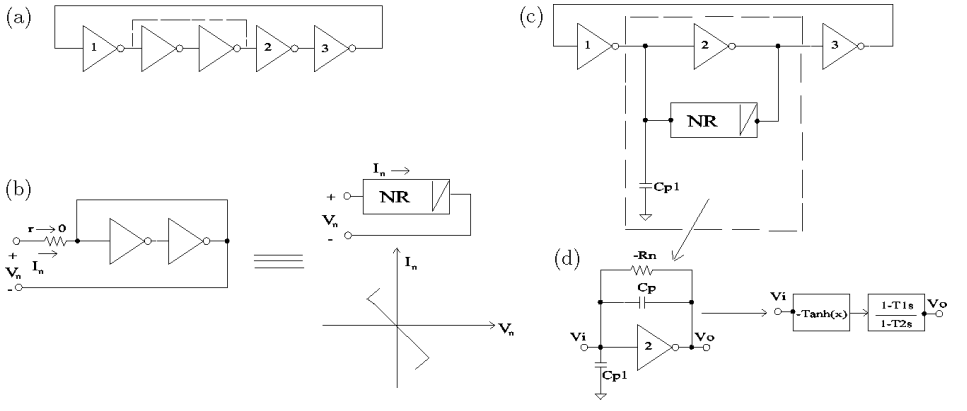

Fig. 6. Five-stage ring oscillator with one-short circuit and its nonlinear model.

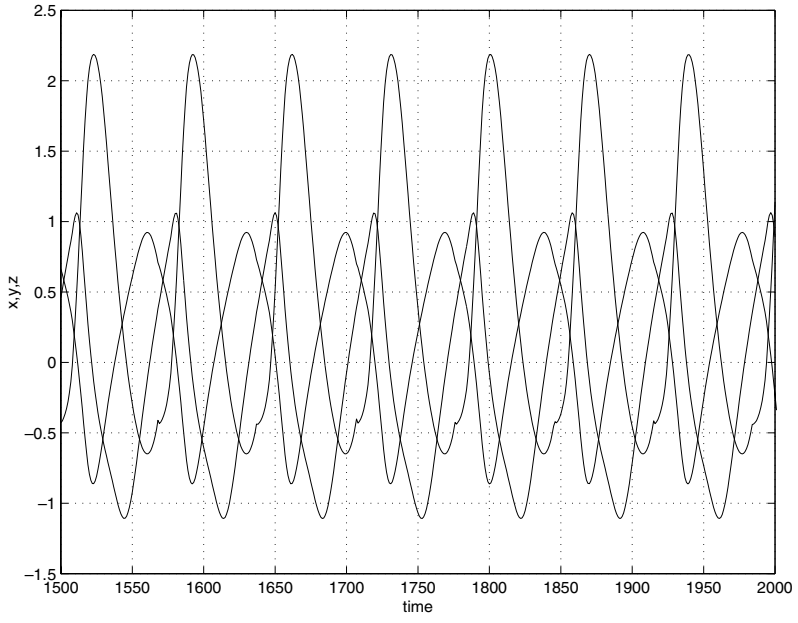

(a)

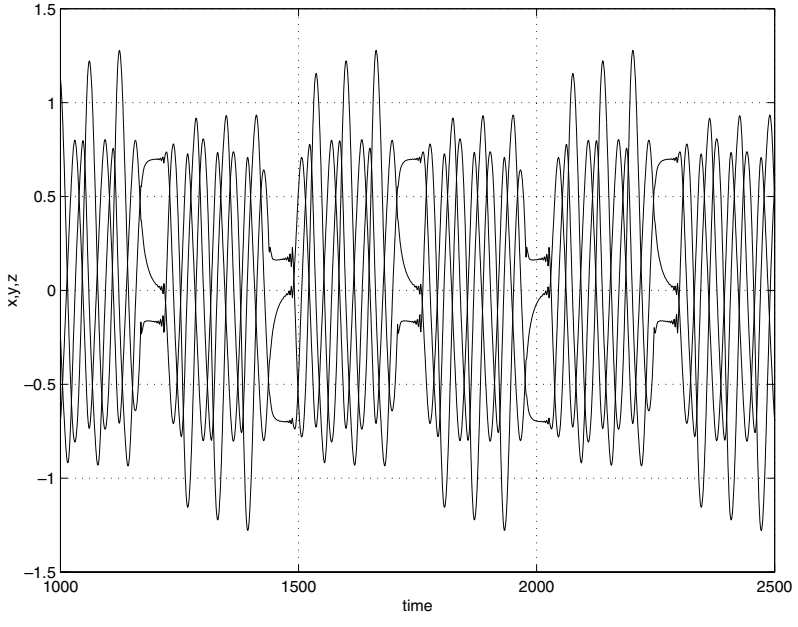

(b)

Fig. 7. Simulation results of the 5-stage ring oscillator with one short (a) periodic oscillations, (b) chaotic oscillations and (c) chaotic attractor.

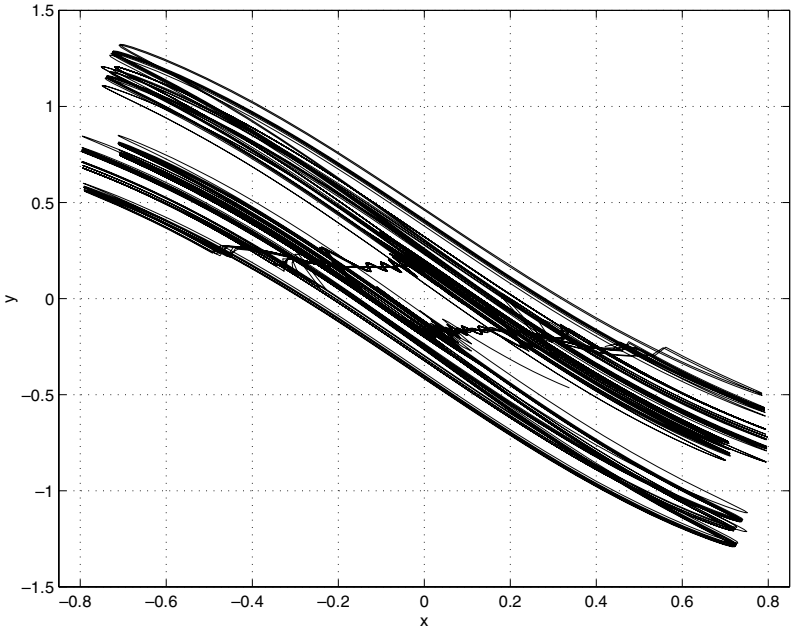

(c)

Fig. 7. (*Continued*)

Figure 7(a) shows the waveforms obtained from this model with $\alpha = 1.05$, $\beta = 1$, $k_1 = 30$ and $k_2 = 15$. The waveforms are oscillatory although not sinusoids. Figure 7(b) shows the waveforms with $k_1 = 20$; these waveforms are chaotic and the chaotic attractor is shown in Fig. 7(c) in the $x - y$ phase plane.

4. Conclusion

We have proposed nonlinear models for three- and five-stage ring oscillators with some practical special cases also considered. Findings of particular importance are:

- The necessary loop gain required to start oscillations was found to be not only $A = -1$ but also $A = +1$ with the implication that ring oscillators can be realized via cascaded "special buffers" rather than inverters. The normalized oscillation frequency ω_o equals either $\sqrt{n}$ or $1/\sqrt{n}$ (n is the number of cascaded stages) depending on which oscillation condition is chosen.
- The practical five-stage ring oscillator with two shorts, known to reduce noise content, was explained in terms of effective system order. Hysteresis and latch-up in this oscillator were also shown to be possible.
- The performance of a five-stage ring oscillator with one short was analyzed. This oscillator can be driven into chaotic oscillation mode.

References

1. A. Hajimiri, S. Limotyrakis and T. Lee, Jitter and phase noise in ring oscillators, *IEEE J. Solid-State Circuits* **34** (1999) 790–804.
2. M. Grozing, B. Philipp and M. Berroth, CMOS ring oscillator with quadrature outputs and 100 MHz to 3.5 GHz tuning range, *Proc. European Conf. Solid-State Circuits, ESSCIRC 03*, Portugal (2003).
3. Y. Eken and J. Uyemura, A 5.9 GHz voltage-controlled ring oscillator in 0.18 μm CMOS, *IEEE J. Solid-State Circuits* **39** (2004) 230–233.
4. A. S. Elwakil, Explaining hysteresis in electronic circuits, *Int. J. Electr. Eng. Education* **43** (2006) 252–260.
5. A. S. Elwakil and S. Ozoguz, Explaining hysteresis in electronic circuits: Robust simulation and design examples, *Proc. IEEE Int. Conf. Electronics, Circuits and Systems ICECS'06*, Nice, France (2006), pp. 244–247.
6. A. S. Elwakil and W. M. Ahmed, On the necessary and sufficient conditions for latch-up in sinusoidal oscillators, *Int. J. Electron.* **89** (2002) 197–206.
7. M. P. Kennedy, Chaos in the Colpitts oscillator, *IEEE Trans. Circuits Syst.-I* **41** (1994) 771–774.
8. O. De Feo and G. Mario, Bifurcations in the Colpitts oscillator: From theory to practice, *Int. J. Bifurc. Chaos* **13** (2003) 2917–2934.
9. A. S. Elwakil, Explaining latchup in a classical Wien oscillator, *Analog Integr. Circuits Signal Process.* **48** (2006) 239–245.
10. S. Lee, B. Kim and K. Lee, A novel high-speed ring oscillator for multiphase clock generation using negative skewed delay scheme, *IEEE J. Solid-State Circuits* **32** (1997) 289–291.
11. K. O'Donoghue, M. P. Kenendy and P. Forbes, A fast and simple implementation of Chua's oscillator using a cubic-like Chua diode, *Proc. Euro. Conf. Circuit Theory and Design ECCTD'05*, Vol. 2, Cork, Ireland (2005), pp. 83–86.
12. V. Srinivasan, S. Islam and B. Blalock, Minimizing phase noise variation in CMOS ring oscillators, *Analog Integr. Circuits Signal Process.* **34** (2003) 259–263.
13. L. O. Chua and P. M. Lin, *Computer-Aided Analysis of Electronic Circuits* (Prentice-Hall, Englewood Cliffs, 1975).
14. M. P. Kennedy and L. O. Chua, Hysteresis in electronic circuits: A circuit theorist's perspective, *Int. J. Circuit Theory Appl.* **19** (1991) 471–515.
15. L. Chua, C. Desoer and E. Kuh, *Linear and Nonlinear Circuits* (McGraw-Hill, 1987).